Influence of defects on the order-disorder phase transition of a Si(001) surface

Yoshimichi Nakamura, Hiroshi Kawai, and Masatoshi Nakayama*
Department of Physics, Faculty of Science, Kyushu University, Ropponmatsu, Fukuoka 810, Japan
(Received 15 July 1996)

We study the influence of surface defects on the order-disorder phase transition of a Si(001) surface using Monte Carlo (MC) simulations based on the asymmetric-dimer model. The transition becomes broad in the system with a low density of the type-C defect. The temperature dependence of the long-range-order parameter (LOP), local-order parameter, and the intensity of the low-energy electron diffraction (LEED) peak is investigated. In order to analyze the local ordering from the scanning-tunneling-microscopy (STM) image quantitatively, the fraction of the site of the asymmetric image, called ''mesoscopic ordering index'' (MOI), is introduced. The critical temperatures, defined as the middle point of the transition region of the LOP, the MOI, and the LEED intensity, are almost the same. The experimental temperature dependence of the LEED peak is explained by a combined effect of the defects and the coherence length. The present study offers an answer to the question what actually corresponds to the transitions observed in LEED and STM experiments. [S0163-1829(97)07116-6]

I. INTRODUCTION

A reconstruction based on the formation of the dimers has been widely accepted on Si(001) surface. Earlier calculations[1] predicted that an asymmetric dimer is more stable than a symmetric one. Recent first-principles calculations[2–4] have shown that the ground state of the Si(001) surface is the $c(4\times2)$ structure with the asymmetric dimers. The structure turns into a disordered state through an order-disorder phase transition.[2–4]

Early low-energy electron diffraction (LEED) experiments at room temperature[5] showed that Si(001) surface is reconstructed to a (2×1) structure. Precise measurement of the LEED patterns was performed by Tabata, Aruga, and Murata.[6] They observed the quarter-order spots characteristic to the $c(4\times2)$ structure at low temperature. They found that as the temperature increases, the LEED intensity of the quarter-order spot drops in the transition region 150–250 K. The full width at half maximum of the quarter-order spot is constant at low temperature but begins to increase at about 200 K, which is almost the middle point of the transition region. It has been confirmed that the transition from the $c(4\times2)$ to the (2×1) structure at about 200 K is an order-disorder transition with respect to the arrangement of the asymmetric dimers.

In scanning-tunneling-microscopy (STM) images observed by Hamers, Tromp, and Demuth,[7] symmetric-appearing images exhibiting the (2×1) structure are seen in most part of the surface at room temperature except near defects or step edges. In the first low-temperature STM images by Wolkow,[8] the asymmetric images of the $c(4\times2)$ structure are seen to a large extent (60–80% of the surface), while a large area of symmetric-appearing images still remains in a region of low defect density. Tochihara, Amakusa, and Iwatsuki[9] observed by low-temperature STM a broad single domain of the $c(4\times2)$ structure with the asymmetric images. STM images have been used only qualitatively to detect the change of the ordering of a local region in the study of the phase transition. The critical temperature for the transition of the surface has not been determined from the STM experiments.

Inoue *et al.*[2–4] have studied the order-disorder phase transition on Si(001) surface by using Monte Carlo (MC) simulations based on the asymmetric-dimer model. In their calculation, the real system is mapped onto an Ising spin system by assuming that the two possible orientations of the asymmetric dimer correspond to the two degrees of freedom of an Ising spin. The values of the coupling constants are derived from results of their first-principles total-energy calculations.[2–4] They found that the structural phase transition occurs at about 320 K in the defect-free system. A qualitative discrepancy is seen between the theoretical result[2–4] and the experimental one[6] in the sharpness of the phase transition. The transition range is found to be broad in the experiment, while very narrow in the MC simulation. They found that the phase transition is much affected by a small amount of model defects. The broad transition region observed experimentally has been attributed to the presence of defects on the real surface. However, the temperature dependence of the LEED intensity is not reproduced well in their calculations.[2–4] They did not analyze STM images.

In the present paper we investigate how the LEED intensity and STM images change with temperature on the basis of MC simulation. We perform MC simulations in the system with a low density of the type-C defect[10] that is actually seen on the real surface.[9] We examine the temperature dependence of the long-range-order parameter (LOP) and the local-order parameter defined in the MC simulation. We propose the fraction of the site of the asymmetric image, called ''mesoscopic ordering index (MOI),'' to describe the change of the ordering of a local region. We see that the temperature dependence of the MOI gives the change of the ordering in terms of STM images quantitatively. We examine in detail the temperature dependence of the LEED intensity. We take into account the effect of the coherence length of the incident electron beam. We estimate the critical temperature from the middle point of the transition region of the LOP, the MOI, and the LEED intensity, and results are compared. We see

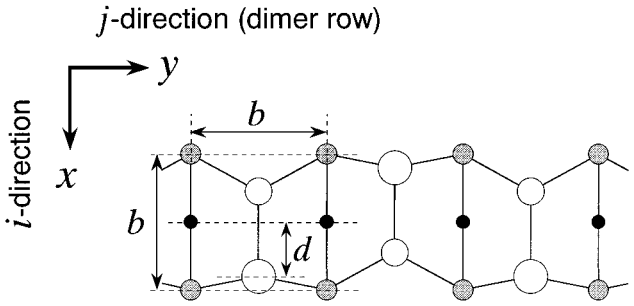

FIG. 1. Top view of the Si(001) surface structure. Open, shaded, and black circles denote the surface-, second-, and third-layer atoms, respectively. Larger and smaller open circles correspond to the up- and down-atom of each dimer, respectively. $b=a/\sqrt{2}$ (a is the bulk lattice constant). The ratio d/b ($=0.34$) is determined by the first-principles calculation (Refs. 2–4).

that the experimental temperature dependence of the LEED peak[6] is explained as a combined effect of the defects and the coherence length.

II. MODEL AND METHOD

First we consider the model of the defect free surface. Our calculations are based on the asymmetric-dimer model in which each dimer buckles with respect to the surface and lines up the row (Fig. 1). The tilting angle is assumed to take only two values θ_0 and $-\theta_0$. This model is adequate to describe the arrangements of the dimers and the flip-flop motions. The model is described by the Ising spin Hamiltonian,

$$H=V\sum_{i,j} S_{i,j}S_{i,j+1}+H\sum_{i,j} S_{i,j}S_{i+1,j}$$

$$+D\sum_{i,j} S_{i,j}(S_{i+1,j-1}+S_{i+1,j+1}), \qquad (1)$$

where $S_{i,j}=\pm 1$ corresponds to the angle $\pm\theta_0$ at the site (i,j) defined in Fig. 2. The coupling constants are illustrated in Fig. 2. The values are determined from the first-principles energy calculations by Inoue and co-workers,[2–4]

$$V=51.9 \text{ meV}, \quad H=-6.6 \text{ meV}, \quad D=-3.6 \text{ meV}. \qquad (2)$$

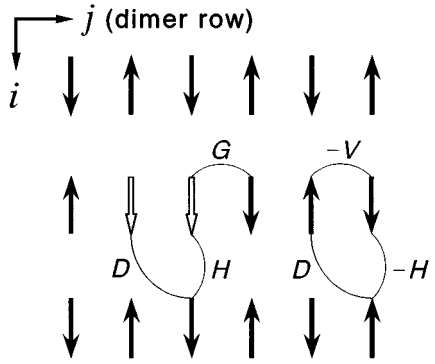

FIG. 2. Arrangement of asymmetric dimers represented by Ising spins. The two neighboring open arrows represent defect spins of the type-C defect. The values of the coupling constants are given in the text.

The ground state of the Hamiltonian is the asymmetric $c(4\times 2)$ structure.

Inoue and co-workers[2–4] have studied influence of defects on the structural phase transition on Si(001) using model defects in MC simulations based on the Ising spin model. In their calculations, the defect is assumed to be of single site type. The two spins next to the defect along the dimer row are fixed in either parallel or antiparallel to each other.

As we see in the actual STM images,[9] the type-C defect influences the ordering of the nearby dimers. The STM image of the type-C defect is two neighboring protrusions on one side of the dimer row. The defect plays the role of the phase shifter.[9] Recently, the ground state of the type-C defect has been investigated by first-principles energy calculations.[11,12] According to their result, an atom is missing in the second surface layer and the two neighboring atoms on the first layer indeed protrude. The up atom and the down atom of the dimer are practically at about the same position as those of the perfect $c(4\times 2)$ structure. Therefore, we represent the defect by a fixed pair of parallel spin[13] ($S_{i,j}=S_{i,j+1}=\pm 1$) as shown in Fig. 2. The coupling of the defect spin to the neighboring rows is assumed to be the same as the host (Fig. 2). The coupling constant of the defect spin to the nearest neighbor along the dimer row is defined as G. In our previous simulations,[13] we successfully reproduced the influence of the isolated type-C defect observed by STM both at low and at high temperature.[9]

In the present study, we perform MC simulation for a system with the type-C defects of a low density to study the effect on the order-disorder transition. We perform Monte Carlo (MC) simulations on the system of $N=40$ (dimer rows)$\times 400$ (dimers), employing periodic boundary conditions. The Metropolis algorithm is used for updating spin configuration. At each temperature, a number of the first MC steps are required to ensure equilibration. Then the following MC steps are used to calculate thermodynamic averages.

We define the local-order parameter for the $c(4\times 2)$ structure as follows:

$$P(i,j)=(-1)^{i+j}\langle S_{i,j}\rangle, \qquad (3)$$

where the brackets $\langle\cdots\rangle$ denote the average over MC steps. There are two domains of the $c(4\times 2)$ structure. The site (i,j) is defined to belong to the $(\pm)$ phase when $(-1)^{i+j}S_{i,j}=\pm 1$. The probability that the site (i,j) belongs to the $(\pm)$ phase $P_{\pm}(i,j)$ is expressed as follows:

$$P_{+}(i,j)=\frac{1+P(i,j)}{2},$$

$$P_{-}(i,j)=1-P_{+}(i,j). \qquad (4)$$

The LOP for the $c(4\times 2)$ structure is defined as

$$\langle\psi\rangle=\sum_{i,j} P(i,j)/N, \qquad (5)$$

where N is total number of the spins ($N=N_i\times N_j$).

STM images are approximated by the superposition of the image from the up-atom in each dimer at site (i,j). When the site (i,j) belongs to the $(\pm)$ phase, the coordinate of the

up-atom is $(x,y)=[2ib\pm(-1)^{i+j}d,jb]$ on the surface, as shown in Fig. 1. In view of the calculated local density of states,[14] we approximate STM images by superposition of the image due to contribution from the dangling-bond orbital of the up-atom.[13] Assuming that the image from the up atom is represented by a two-dimensional Gaussian function with the extent σ, we can get the intensity $I(x,y)$ in terms of $P(i,j)$,

$$I(x,y)=\frac{1}{\pi\sigma^2}\sum_{i,j}\left[P_+(i,j)\exp\left(-\frac{\{x-[2ib+(-1)^{(i+j)}d]\}^2+(y-jb)^2}{\sigma^2}\right)+P_-(i,j)\right.$$
$$\left.\times\exp\left(-\frac{\{x-[2ib-(-1)^{(i+j)}d]\}^2+(y-jb)^2}{\sigma^2}\right)\right]. \quad (6)$$

We calculate the LEED intensity based on kinematical theory from the MC simulations. Since the interaction time of the incident electron with the surface is much shorter than that of the flip-flop motion, the intensity is calculated for each snapshot and the average is taken thereafter. The LEED intensity depends on both the long-range and short-range order. The intensity remains finite even in the disordered phase, because a small area of the $c(4\times2)$ structure is formed locally and temporally. Another point is that in real experiments each electron interacts with a finite area where the coherence of the electron wave is kept. The coherence length, the linear dimension of the area, is typically 100–200 Å. In the previous LEED calculations from the MC simulations by Inoue *et al.*,[2–4] the incident wave is assumed to be coherent over the total rectangular area employed in the simulation (about 150 Å$\times$2000 Å). To study the effect of the coherence length, we calculate the LEED intensity by assuming that the coherence is kept over squares of several size. The coherence length is represented by the side of the square, which is denoted by $20\,bm$ ($m=1$, 2, 3 and 4), where $b=a/\sqrt{2}$ (a is the bulk lattice constant). $m=1$, 2, 3, and 4 corresponds to about 80, 160, 240, and 320 Å, respectively. For each m, the LEED intensity is given by a moving average of the contributions from all the square regions. The LEED intensity for (3/4, 1/2) spot with coherence length m is proportional to the quantity

$$I=\frac{1}{m^2}\left\langle\left\langle\left|\sum_{i,j}S_{i,j}\exp[i(3i+j)\pi]\right|^2\right\rangle_{\mathrm{MC}}\right\rangle_{\text{moving AVR}}, \quad (7)$$

where the sum is over the square region of m. $\langle\cdots\rangle_{\mathrm{MC}}$ and $\langle\cdots\rangle_{\text{moving AVR}}$ denote the average over the MC steps and the moving average over the squares, respectively. We call the dependence of the LEED intensity on the coherence length m as ''m dependence.''

III. RESULTS

We assume $G=40$ meV.[13] The defect density is assumed to be 1% and the defects are distributed randomly (referred to as 1% type-C defect case). At each temperature, the first $10^4-1.5\times10^5$ MC steps are required to reach the equilibrium state. The following $10^4-3.0\times10^5$ MC steps are used to calculate thermodynamic averages.

A. Long-range-order parameter (LOP)

We show in Fig. 3 the result of the temperature dependence of the long-range-order parameter (LOP). At each temperature the mean value is estimated from the total MC steps for the thermodynamic average and the standard deviation is shown as the error bar in the figure.

Figure 3(a) shows the result of the defect-free system. $\langle\Psi\rangle$ fluctuates around zero at high temperature. When the tem-

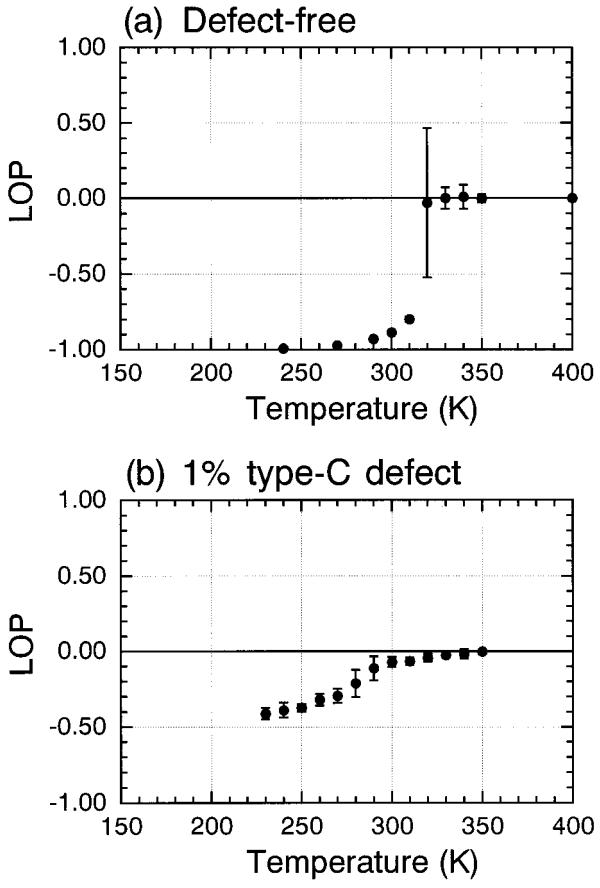

FIG. 3. Temperature dependence of the long-range-order parameter (LOP). (a) The defect-free system. (b) The 1% type-C defect case.

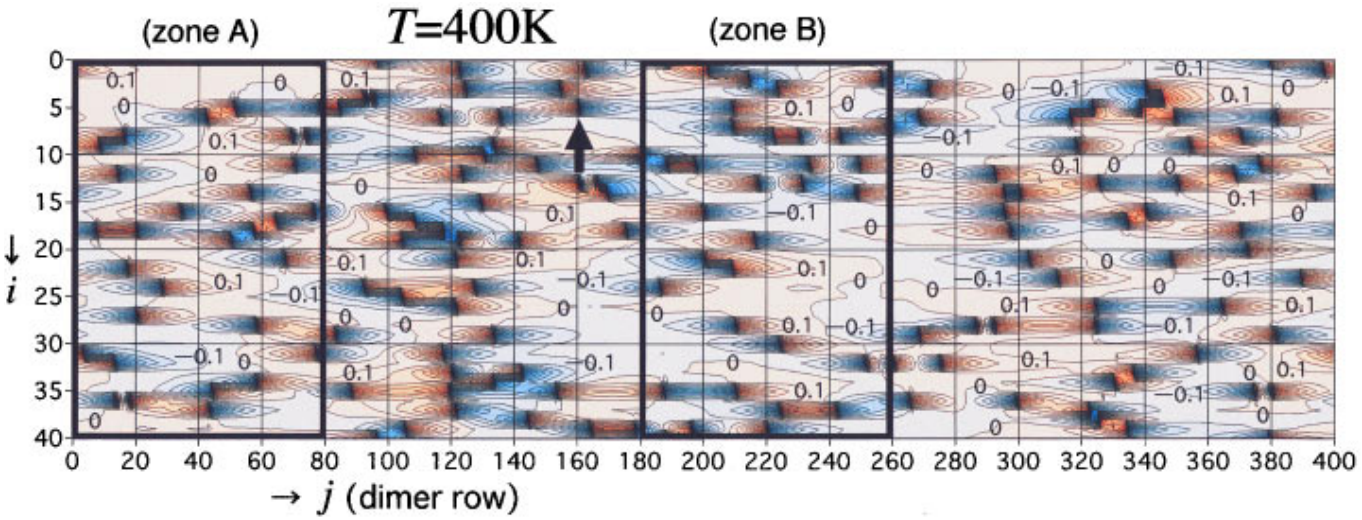

FIG. 4. Contour map of the local-order parameter $P(i,j)$ at $T=400$ K for the 1% type-C defect case. Lines are drawn for the interpolated values of $P(i,j)$ with the interval 0.1. As an example, the position of one of the type-C defects [a pair of the defect spins at (5,160) and (5, 161)] is indicated by an arrow. The squares of coherence length $m=1$ are shown by the rectangles of 20(dimers)×10(dimer rows) in the figure.

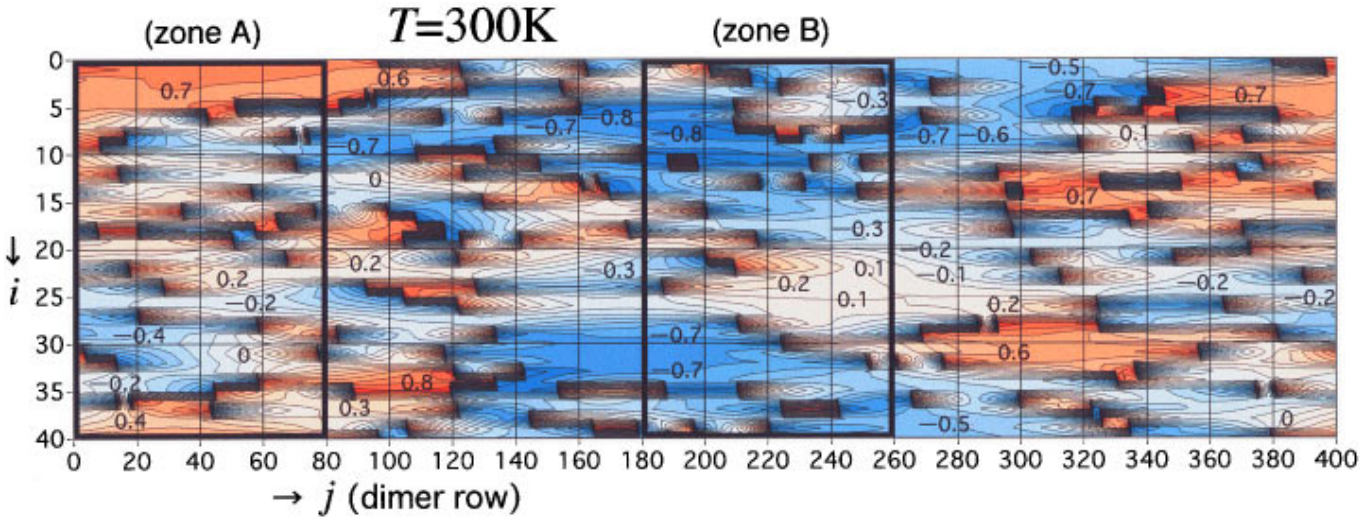

FIG. 5. Contour map of the local-order parameter $P(i,j)$ at $T=300$ K for the 1% type-C defect case. Lines are drawn for the interpolated values of $P(i,j)$ with the interval 0.1. The squares of coherence length $m=1$ are shown by the rectangles of 20(dimers)×10(dimer rows) in the figure.

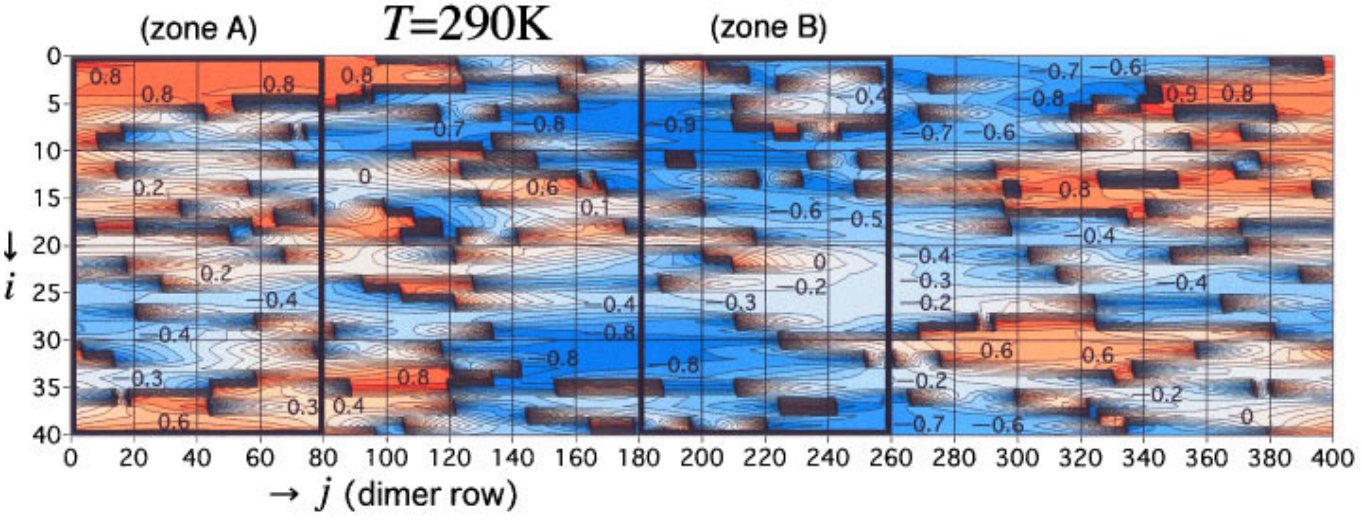

FIG. 6. Contour map of the local-order parameter $P(i,j)$ at $T=290$ K for the 1% type-C defect case. Lines are drawn for the interpolated values of $P(i,j)$ with the interval 0.1. The squares of coherence length $m=1$ are shown by the rectangles of 20(dimers)×10(dimer rows) in the figure.

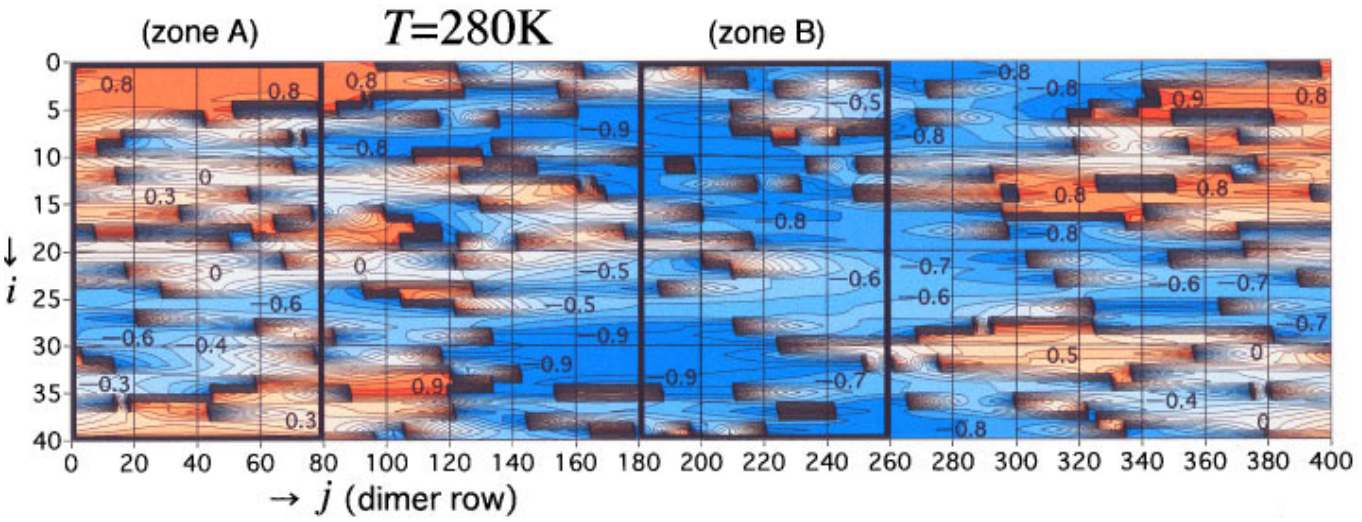

FIG. 7. Contour map of the local-order parameter $P(i,j)$ at $T=280$ K for the 1% type-C defect case. Lines are drawn for the interpolated values of $P(i,j)$ with the interval 0.1. The squares of coherence length $m=1$ are shown by the rectangles of 20(dimers)×10(dimer rows) in the figure.

perature is lowered through 320–310 K, the absolute value of $\langle\Psi\rangle$ increases rapidly to almost unity. The structure changes into the ordered $c(4\times2)$ structure. We define the critical temperature T_C(LOP) as the middle point of the transition region of the LOP. From Fig. 3(a), T_C(LOP) is determined to be about 320 K, which is almost the same as the previous theoretical result.[2–4]

Figure 3(b) shows the result of the 1% type-C defect case. $\langle\Psi\rangle$ is reduced to be about 40% at low temperature. The transition region becomes broad and shifts to lower side as compared with that of the defect-free system. These features are similar to the result of the system with 1% defects by Inoue and co-workers.[2–4] From Fig. 3(b), the critical temperature T_C(LOP) is determined to be about 290 K.

B. Contour map of the local-order parameter and STM image

There are two domains for the $c(4\times2)$ structure. At finite temperature the direction of the spin fluctuates between the two directions. We call that a particular site belongs to (+) or (−) region on the average in accordance with the sign of the local-order parameter $P(i,j)$ defined by Eq. (3). The contour maps of $P(i,j)$ are shown for $T=400$ K (Fig. 4), 300 K (Fig. 5), 290 K (Fig. 6), 280 K (Fig. 7), and 230 K (Fig. 8). In these figures the (+) and (−) domains are shown in red and blue, respectively. STM images can be calculated approximately in terms of $P(i,j)$ by Eq. (6).[13] Calculated STM images are practically asymmetric when $|P(i,j)|\geqslant0.3$. Thus the regions can be classified as follows: (a) (+) asymmetric [$P(i,j)\geqslant0.3$; high red], (b) symmetric [$|P(i,j)|<0.3$; faint red or blue], (c) (−) asymmetric [$P(i,j)\leqslant-0.3$; high blue]. In the symmetric region, spins are fluctuating frequently as the domain boundary moves rapidly from one snapshot to the other.

At high temperature, the system is in disordered phase and $P(i,j)$ takes small values in most part of the system [Fig. 4 ($T=400$ K)]. $P(i,j)$ takes large magnitude only in

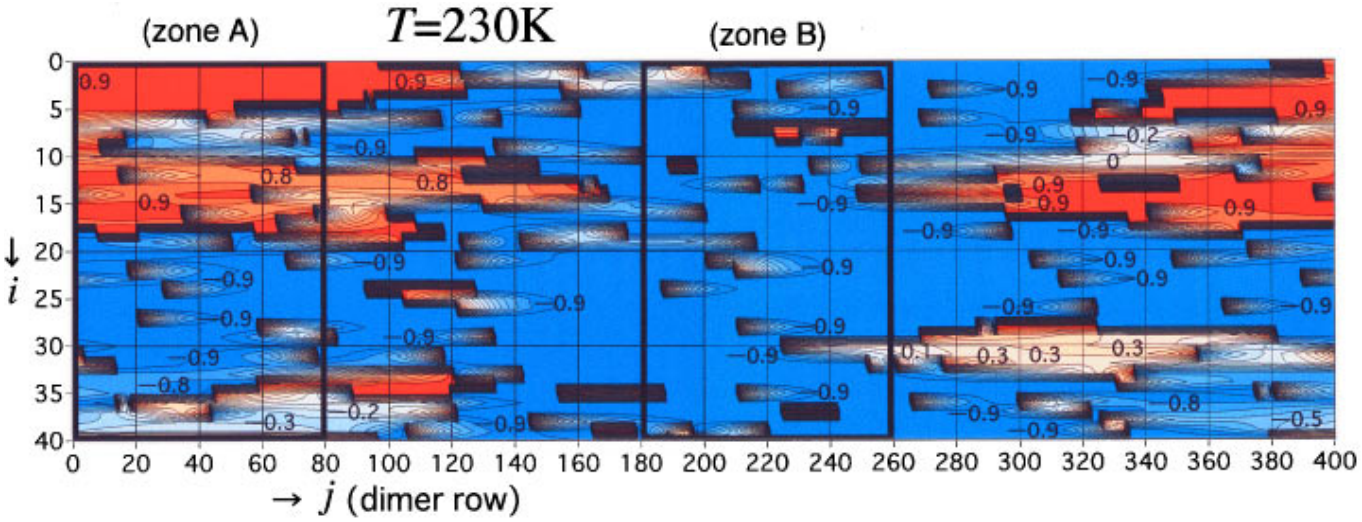

FIG. 8. Contour map of the local-order parameter $P(i,j)$ at $T=230$ K for the 1% type-C defect case. Lines are drawn for the interpolated values of $P(i,j)$ with the interval 0.1. The squares of coherence length $m=1$ are shown by the rectangles of 20(dimers)×10(dimer rows) in the figure.

the vicinity of each defect. When we calculate the STM image, we see that each defect induces the asymmetric images on both the sides with almost equal length but opposite phase. This is what has been observed in room temperature experiment[9] as a characteristic feature of the type-C defect.

The influence of the defects becomes longer as the temperature decreases. Each defect competes or cooperates with nearby defects according to their mutual configurations [Fig. 5 ($T=300$ K), Fig. 6 ($T=290$ K), Fig. 7 ($T=280$ K)]. At $T=230$ K, the system is divided into several patches of domains with large magnitude of $P(i,j)$ (Fig. 8). The structure of the domains vary from one local region to the other. Asymmetric regions of both the phases coexist in the region of $1\leqslant i\leqslant 40$, $1\leqslant j\leqslant 80$ (referred to as ''zone A'' enclosed by the bold lines in Fig. 8). A single domain of $(-)$ phase dominates almost completely over the region of $1\leqslant i\leqslant 40$, $181\leqslant j\leqslant 260$ (referred to as ''zone B'' enclosed by the bold lines in Fig. 8). $P(i,j)$ takes small values locally on only one side of most of the type-C defects in the zone B. Few numbers of the symmetric-appearing images of the dimers are to be seen there when we calculate STM images. This feature is essentially the same as that of the low-temperature STM image observed by Tochihara, Amakusa, and Iwatsuki (Fig. 2 in Ref. 9). We see in Fig. 8 that a single domain of $(+)$ phase dominates over the region of $1\leqslant i\leqslant 20$, $340\leqslant j\leqslant 60$ (referred to as ''zone C'').

There are a few numbers of wide regions with rather low defect densities where $P(i,j)$ takes small values, e.g., the region of $25\leqslant i\leqslant 35$, $220\leqslant j\leqslant 380$ (referred to as ''zone D'') and that of $35\leqslant i\leqslant 40$, $20\leqslant j\leqslant 120$ (referred to as ''zone E'') in Fig. 8. In these regions the influence of the defects is much wider than the simple sum of the isolated defects. Several tens of the symmetric-appearing images of the dimers are to be seen there when we calculate STM image. However, the nature of the large symmetric region is different between zone D and E. In zone E the large symmetric region is seen between the two domains of opposite phase in zone A. In zone D, on the other hand, the large symmetric region is surrounded by a single domain. The latter feature is essentially the same as that of the low-temperature STM image observed by Wolkow (Fig. 2 in Ref. 8). In our previous paper,[13] we found that in a particular configuration of four type-C defects, the influence of the defects is much wider than the simple sum of the isolated defects. We find that such effects indeed appear when the defects are distributed randomly with a low defect density. When the temperature further decreases, spins in zone D and E will be fixed to form the ground state, which might have an inhomogeneous structure within the region. Therefore, the total system will be divided into the $(+)$- and the $(-)$-asymmetric regions at 0 K.

We have seen completely different influence of the type-C defects between zone B and D surrounded by a single domain in accordance with the configuration of the defects in each zone. This implies that different features of the low-temperature STM image by Tochihara, Amakusa, and Iwatsuki[9] and by Wolkow[8] can be observed on the same surface.

C. Mesoscopic ordering index

STM images have been used only qualitatively to detect the change of the ordering of a local region in the study of the phase transition. Each dimer reveals asymmetric or symmetric-appearing in actual STM image. It is difficult to derive the value of $P(i,j)$ directly from the STM image. We introduce the fraction of the asymmetric images of each phase, Q_+ and Q_-, as a measure to describe the ordering of a mesoscopic scale. We call (Q_+,Q_-) a mesoscopic ordering index (MOI). The MOI can be obtained from the observed STM image by simply counting the number of the asymmetric dimers. In the present MC simulation, we know that the asymmetric images of $(+)$ and $(-)$ phase correspond to $P(i,j)\geqslant 0.3$ and $P(i,j)\leqslant -0.3$, respectively.[13] Q_+ and Q_- represent the ordering in a local region on a coarse grained scale. We calculate the temperature dependence of Q_+ and Q_- to illustrate its effectiveness in the quantitative analysis of the ordering from the STM image.

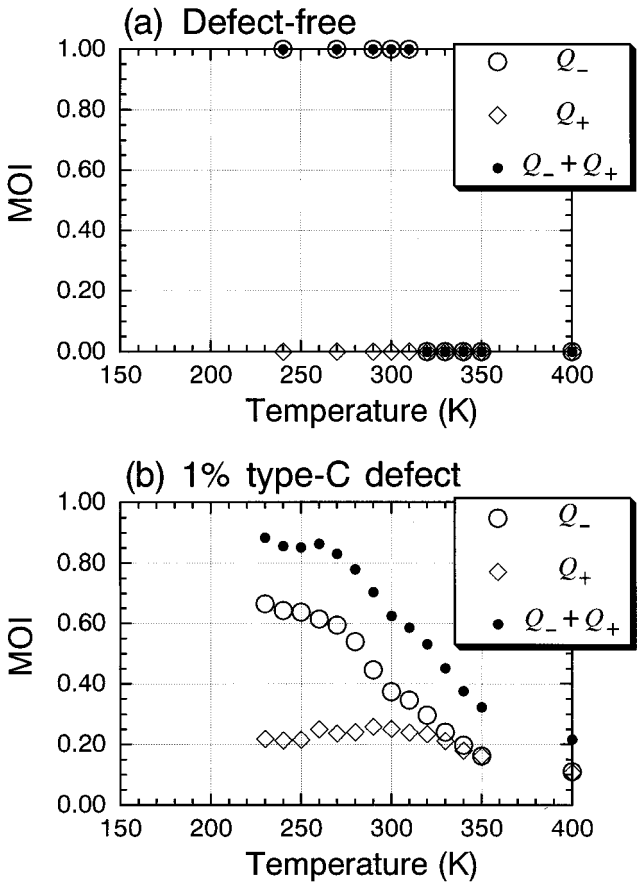

FIG. 9. Temperature dependence of Q_-, Q_+, and $Q_+ + Q_-$. (a) The defect-free system. (b) The 1% type-C defect case.

We show in Fig. 9 the temperature dependence of Q_-, Q_+, and $Q_+ + Q_-$. In the case of the defect-free system [Fig. 9(a)], Q_+, Q_-, and $Q_+ + Q_-$ are almost zero at high temperature. When we calculate STM images, the symmetric-appearing images are to be seen all over the system. As the temperature decreases below 320 K, only Q_- increases to be almost 1. When we calculate STM images, the single domain of the $c(4\times 2)$ structure [$(-)$ phase] with asymmetric-appearing images is to be seen in almost all the system. We define for the general case the critical temperature $T_C(Q_+)$ and $T_C(Q_-)$ as the middle point of the transition region of Q_+ and Q_-. From Fig. 9(a), only $T_C(Q_-)$ is

determined to be about 310–320 K, which is almost the same value as the T_C(LOP) for the defect-free system.

In the 1% type-C defect case [Fig. 9(b)], the MOI takes a small but finite value even at high temperature, where Q_+ and Q_- are almost the same. This fact indicates that the asymmetric regions are the simple sum of the contributions from individual defects at high temperature. As we see in our previous calculation,[13] each defect induces the asymmetric images on both the sides with equal length but opposite phase. As the temperature decreases below 340 K, Q_- is slightly larger than Q_+. The difference is ascribed to an interference effect of the neighboring defects, which happens to be slightly in favor for the $(-)$-asymmetric region for the present configuration of the defects.

When the temperature goes down through the transition temperature for the defect-free system (310–320 K), the difference is enlarged, which indicates the onset of the phase transition in local regions. Q_- increases rapidly, while Q_+ tends to saturate around the value 0.22. The temperature dependence of $Q_+ - Q_-$ practically corresponds to that of the LOP [Fig. 3(b)]. Looking into the contour map of $P(i,j)$ at 300 K (Fig. 5), 290 K (Fig. 6), and 280 K (Fig. 7), we notice that a wide region of either sign grows in the area that contains very few defects. The sign of such region is fixed by the configuration of nearby defects. When the effects of the nearby defects are competing, the region remains to be symmetric due to the fluctuating motion of the domain boundary. As the temperature goes down, the order in the $(-)$-asymmetric region becomes stronger and converts nearby symmetric regions into a $(-)$-asymmetric region (230 K, Fig. 8). The conversion will occur at different temperatures depending on the configuration of the defects. Thus the MOI grows gradually as the temperature decreases. From Fig. 9(b), $T_C(Q_-)$ is determined to be about 290 K, which is almost the same as T_C(LOP) for the 1% type-C defect case. $T_C(Q_+)$, on the other hand, cannot be clearly determined from Fig. 9(b).

D. LEED intensity

First, we show the dependence of the peak value of the quarter-order spot on the coherence length, the m dependence, in the defect-free case in Fig. 10(a). In the very high temperature where $\langle\Psi\rangle = 0$ and the short-range order also vanishes, the intensity is of the order 1 and does not depend on m. The intensity gradually increases with the decrease of the temperature because of the development of the short-range order. When the temperature is lowered through 320 K, the intensity increases sharply for each m. The increase is sharper for larger values of m. The reason is that, when $\langle\Psi\rangle$ is not equal to zero, the intensity is almost scaled by the factor $\langle\Psi^2\rangle N$ (N is the number of spins in the coherent region and proportional to m^2). We define the critical temperature T_C(LEED) as the middle point of the transition region of the LEED intensity. From Fig. 10(a), T_C(LEED) is determined to be about 320 K for all m. This is almost the same value of the T_C(LOP) and the $T_C(Q_-)$ for the defect-free system.

Next, we show the temperature dependence of the peak value of the quarter-order spot in the 1% type-C defect case in Fig. 10(b). It shows a much smoother temperature dependence for each m as compared with the defect-free case. The transition region becomes broad and shifts to a lower side. The intensity gradually increases with the decrease of the temperature, and is much reduced as compared with the defect-free case for each m. This corresponds to the suppression of the long-range order by the defects. We find that the transition is seen clearer for larger values of m as well as for the defect-free case. From Fig. 10(b), T_C(LEED) is determined to be about 290 K for all m. This value is almost the same to the T_C(LOP) and the $T_C(Q_-)$ for the 1% type-C defect case.

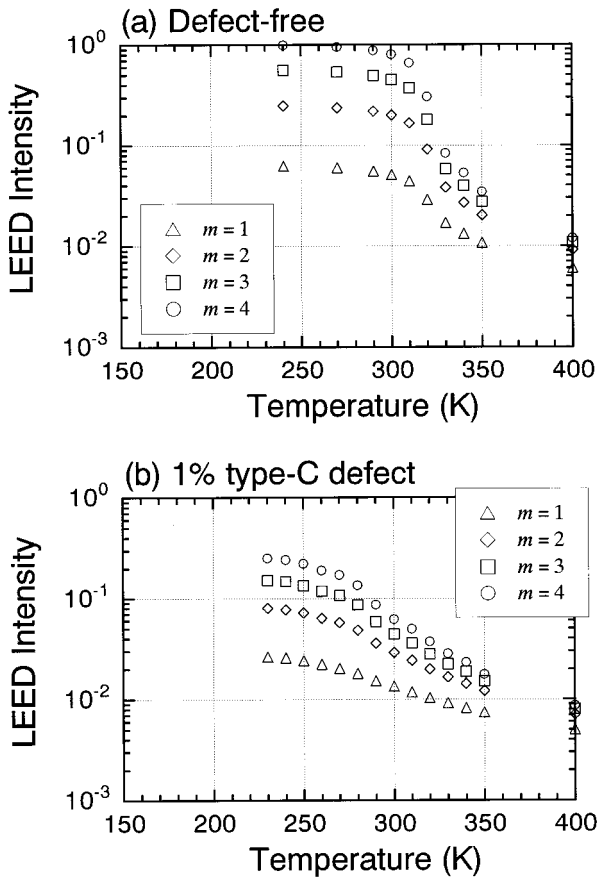

FIG. 10. Temperature dependence of the LEED intensity for a quarter-order spot of the $c(4\times2)$ structure. The intensity is normalized by that with $m=4$ at 240 K for the defect free system. (a) The defect-free system. (b) The 1% type-C defect case.

We compare the result with that of the experiment[6] in Fig. 11. From the experimental data, T_C(LEED) is determined to be about 200 K. The temperature dependence of the LEED intensity obtained from the MC simulation gets closer to the experimental result for smaller values of m. When the result from $m=1$ is shifted to the low temperature side by about 80 K, it agrees well with the experimental result.

IV. DISCUSSION

The present system is an example of random two-dimensional Ising system. According to the rigorous theory of statistical mechanics,[15,16] long-range magnetic order is destroyed by a random magnetic field of nonvanishing strength if the dimension of the system is less than or equal to two. In the present model, we assume that the direction of each de-

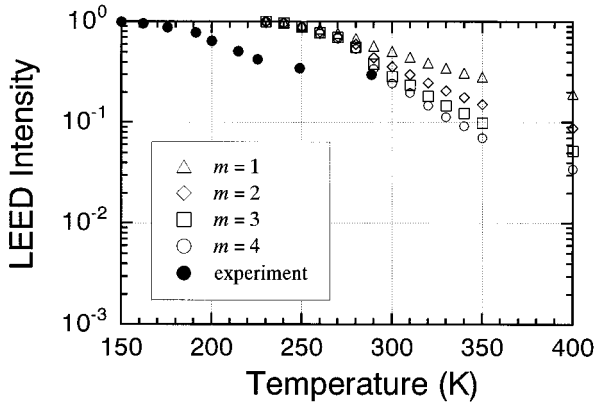

FIG. 11. Temperature dependence of the LEED intensity for a quarter-order spot of the $c(4\times2)$ structure obtained from the MC simulation (the 1% type-C defect case) and the experiment [Ref. 6]. The experimental data are corrected by the Debye-Waller factor. The intensity from the MC simulation is normalized at 230 K. The intensity from the experiment is normalized at 150 K.

fect spin is fixed. This corresponds to the application of the random magnetic field of infinite strength. Therefore, the long-range order must vanish in the strict sense of the word. In the present MC simulation we obtained finite values of the LOP. The reason is of course the finite size of the system employed in the simulation. We have a finite number of defects that take a particular configuration. Since the employed configuration favors the $(-)$-asymmetric region over the $(+)$-asymmetric region, the LOP takes finite values of negative sign. If we look into the subzone of the present system, we notice that the contribution of zone B to the LOP takes a large negative value and dominates the value of the total system. The contribution of zone C is positive. The contribution of zone A is almost zero. In a larger system, the contributions from the subzones like B and C cancel each other out and the LOP tends to zero in the thermodynamic limit. This is what the rigorous theory predicts. Thus the present result does not contradict to the rigorous theory. We note that the real surface should be considered to be a finite system, as it is divided into terraces by the step structure.

In the present simulation, a diffuse transition has been observed in the temperature dependence of the LOP, the MOI, and the LEED intensity. From combined analysis of the contour map of the local-order parameter and the MOI, we find that the ordering proceeds in two stages: (i) growth of asymmetric region around each defect and (ii) growth of asymmetric region of mesoscopic size. As we have seen in the contour map at low temperature (Fig. 8), subsystems of different features, i.e., zone $A,B,\ldots,$ and E appear at the same temperature. This implies that the local phase transition occurs in each region at different temperatures depending on the configuration of the defects.

To see this point we compare, for example, the variations of the contour maps between zone A and B. Local defect densities in zone A and B are about 0.94 and 1.03%, respectively. Completely different behaviors are seen between them. As the temperature decreases, asymmetric regions of both signs grow in zone A (400–280 K, Figs. 4–7). Asymmetric regions coexist with those of opposite sign and symmetric regions at 230 K in zone A (Fig. 8). In zone B, on the other hand, the $(-)$-asymmetric region becomes stronger and converts nearby symmetric regions into the $(-)$ region as shown in the contour maps at 400–230 K (Figs. 4–8). Wide symmetric regions are hardly seen in zone B at 230 K (Fig. 8).

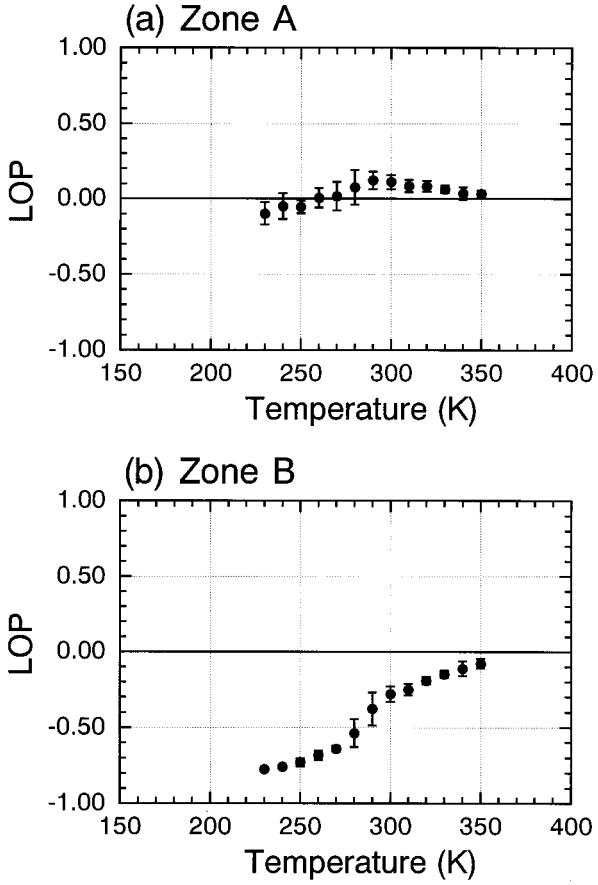

FIG. 12. Temperature dependence of the long-range-order parameter (LOP) of subzones for the 1% type-C defect case. (a) Zone A. (b) Zone B.

We show the temperature dependence of the LOP of zone A and B in Fig. 12(a) and (b), respectively. As the temperature decreases, the LOP of zone A fluctuates around zero. Such a feature is kept as the temperature is lowered to 230 K. On the other hand, the LOP in zone B gradually increases in magnitude as the temperature approaches T_C (LOP) from above. When the temperature is lowered through T_C (LOP), the magnitude increases rapidly, and remains about -0.8 at 230 K. It should be noted that the local defect densities in the two zones are almost the same. This implies that configurations of the type-C defects in each zone have strong influences on the ordering.

We show the temperature dependence of Q_+, Q_-, and $Q_+ + Q_-$ of zone A and B in Fig. 13(a) and (b), respectively. In zone A, Q_+ and Q_- are almost equal at high temperature. As the temperature decreases below 340 K, only Q_+ increases rapidly. This fact indicates that the growth of the $(+)$-asymmetric region of mesoscopic size is seen at first in zone A. The $(+)$-asymmetric region predominates over the $(-)$-asymmetric region for $280\ \mathrm{K} < T < 330\ \mathrm{K}$. Q_-, on the other hand, increases rapidly when the temperature goes down through 300 K, which indicates the onset of the growth

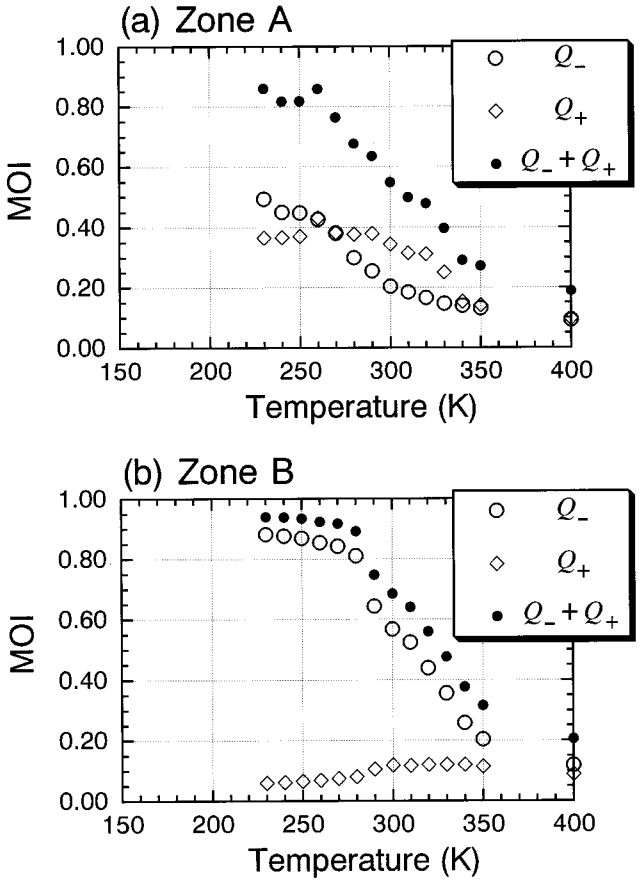

FIG. 13. Temperature dependence of Q_-, Q_+, and $Q_+ + Q_-$ of subzones for the 1% type-C defect case. (a) Zone A. (b) Zone B.

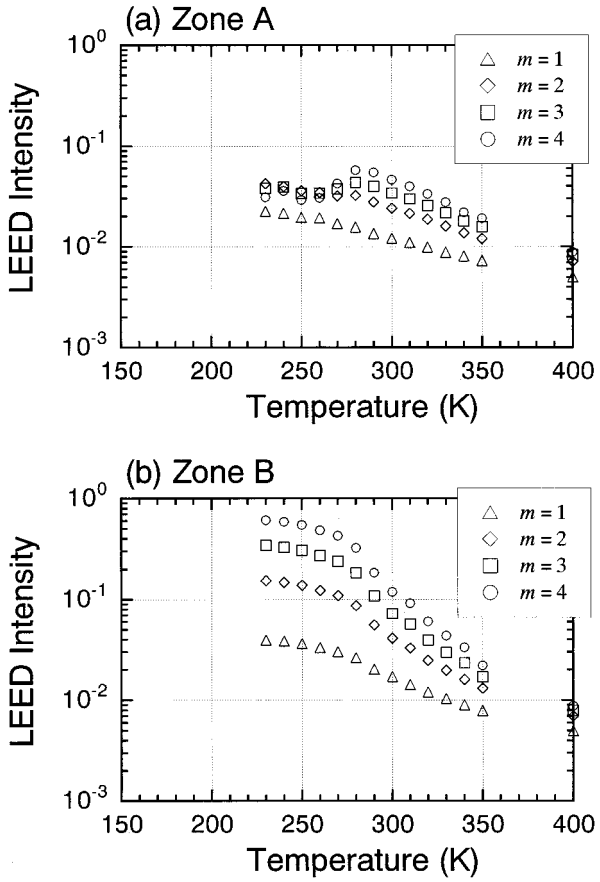

FIG. 14. Temperature dependence of the local LEED intensity of subzones for the 1% type-C defect case. The intensity is normalized by that with $m=4$ at 240 K for the defect-free system. (a) Zone A. (b) Zone B.

of the $(-)$-asymmetric region of mesoscopic size in zone A. The value of Q_- approaches that of Q_+ and at last becomes slightly larger than that of Q_+ below 250 K. From Fig. 13(a), the critical temperature $T_C(Q_+)$ is determined to be about 330 K and $T_C(Q_-)$ about 280 K. Thus the transition of $(\pm)$-asymmetric region is seen clearly from the temperature dependence of the MOI of zone A, though the transition is not seen clearly from that of the LOP. This is an example of effectiveness of the MOI in the quantitative analysis of the transition of subsystem.

Next, we show results of zone B in Fig. 13(b). Q_+ and Q_- are almost the same at high temperature. Q_+ gradually approaches zero as the temperature is lowered down to 230 K, which indicates that the growth of the $(+)$-asymmetric region of mesoscopic size is not seen in zone B. On the other hand, Q_- increases rapidly when the temperature is lowered through 350 K, which indicates the onset of the growth of $(-)$-asymmetric region of mesoscopic size in zone B. The $(-)$-asymmetric region dominates almost completely over zone B at low temperatures. From Fig. 13(b), the critical temperature $T_C(Q_-)$ is determined to be about 310 K. It should be noted that the transition temperature of the $(-)$-asymmetric region differs between zone A (280 K) and zone B (310 K).

We show the m dependence of the local LEED intensity of zone A and B in Fig. 14(a) and (b), respectively. The two zones are significantly different from each other in the temperature dependence of the LOP and that of the contour map. The temperature dependence of the local LEED intensity of zone B [Fig. 14(b)] is almost the same for each m as that of the total system shown in Fig. 10(b). The intensity is several times larger than the average over the total system.

In zone A [Fig. 14(a)], the temperature dependence of the local LEED intensity is completely different from that of the total system [Fig. 10(b)]. The phase transition is not seen clearly for $m \geqslant 3$. Looking into the contour map of zone A at low temperature (Fig. 8), we see domain structures of smaller size as compared with zone B. The transition of each asymmetric region in zone A has been shown by the MOI [Fig. 13(a)]. The formation of mesoscopic ordering in zone A is not clearly observed in LEED with large coherence length. The local intensity of zone A is about a tenth smaller than that of zone B for $m \geqslant 3$. Therefore, contribution to the total LEED intensity from zone A is very small for $m \geqslant 3$. We find that the phase transition is seen only for $m \leqslant 2$ in zone A [Fig. 14(a)]. The intensities of zone A [Fig. 14(a)], of zone B [Fig. 14(b)], and of the total system [Fig. 10(b)] are almost equal for $m=1$. This shows that we can hardly distinguish among the regions with different types of contour maps, e.g., zone A and B, as long as the surface is observed in LEED with short coherence length.

We examine in detail the temperature dependence of the LOP, the MOI and the LEED intensity for local squares of

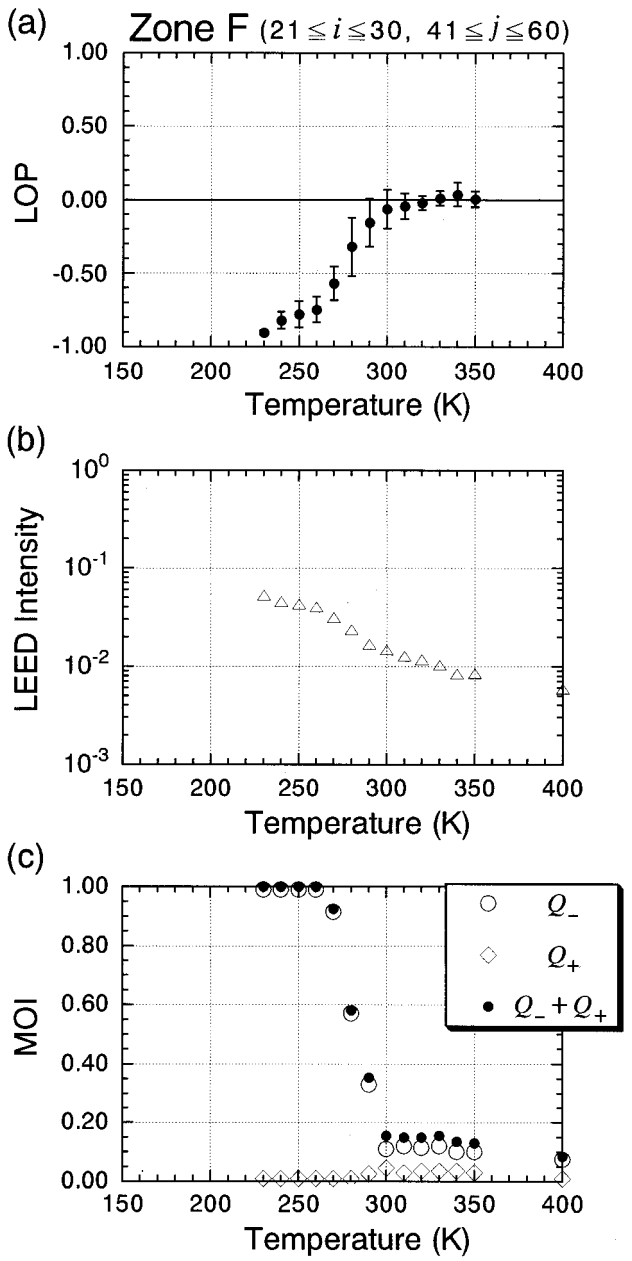

FIG. 15. Temperature dependence of each physical quantity of zone F for the 1% type-C defect case. (a) LOP. (b) Local LEED intensity. (c) Q_-, Q_+, and $Q_+ + Q_-$.

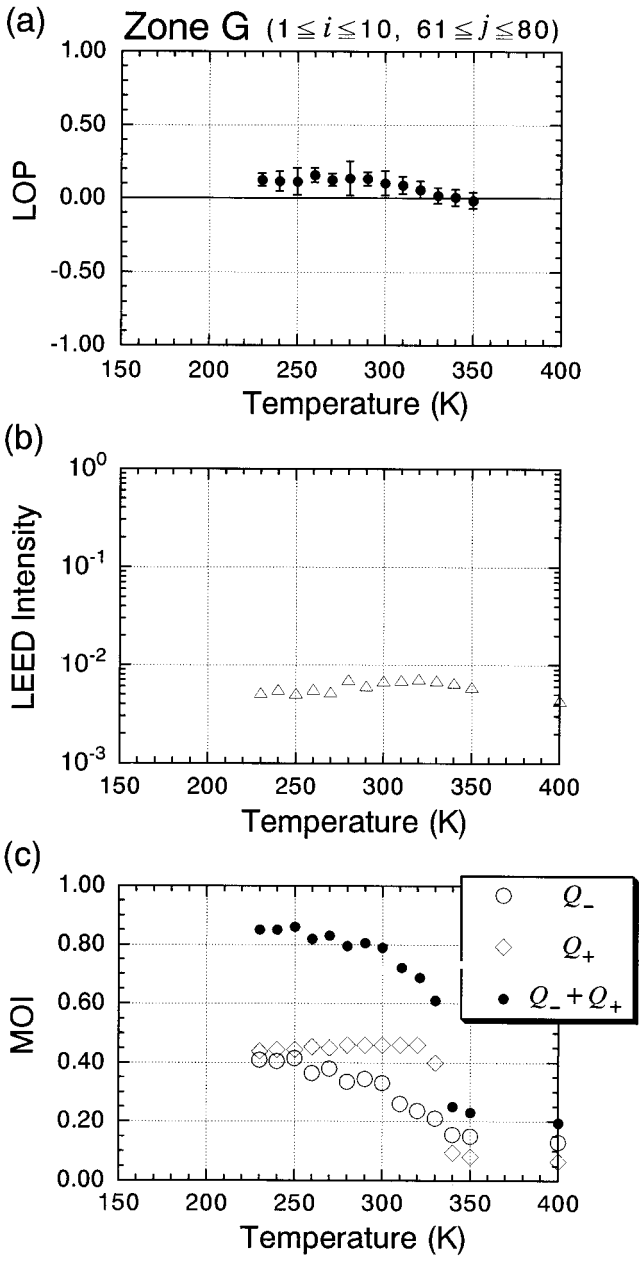

FIG. 16. Temperature dependence of each physical quantity of zone G for the 1% type-C defect case. (a) LOP. (b) Local LEED intensity. (c) Q_-, Q_+, and $Q_+ + Q_-$.

$m=1$ of the present system. We show, for example, results of the local region of $21 \leqslant i \leqslant 30$, $41 \leqslant j \leqslant 60$ (referred to as ''zone F'') and that of $1 \leqslant i \leqslant 10$, $61 \leqslant j \leqslant 80$ (referred to as ''zone G'') in Figs. 15 and 16, respectively. In zone F, the magnitude of the LOP increases rapidly when the temperature is lowered through 290 K [Fig. 15(a)]. The temperature dependence of the LEED intensity shows broad transition region at around 280 K [Fig. 15(b)] in almost the same way as the total system [Fig. 10(b)]. Q_- increases rapidly when the temperature is lowered through 290 K with the transition region much narrower than that of the total system. In zone G, the LOP fluctuates around zero as the temperature decreases [Fig. 16(a)]. The LEED intensity takes very small value in the region 400–230 K [Fig. 16(b)]. The temperature dependence of the LOP and the LEED intensity is much different from those of zone F [Fig. 15(a), (b)]. Q_+ increases abruptly when the temperature is lowered through 340 K [Fig. 16(c)]. Q_- increases in the region 330–250 K to catch up with Q_+ [Fig. 16(c)]. It should be noted that in zone G the transition is clearly seen only by the temperature dependence of the MOI.

The behaviors of the LOP, the MOI, and the LEED intensity of zone G and F are very similar to those of zone A and B, respectively. Both zone $F$and G, having the reduced size, are included in zone A. Thus we see that as we reduce the scale of the observation, we can see how the multidomain zone is composed of the subzones of the single and multidomain types. Abrupt change in the temperature dependence of the MOI indicates the local ordering. The transition becomes sharper with the reduction of the zone scale. However, the

transition temperature differs from one zone to the other reflecting the effect of the configuration of the defects and the ordering of the regions surrounding the zone. We deduce from the above analysis that we can regard a system of enlarged size as an assembly of the multidomain zones of larger size.

We performed MC simulation for another system of 20 $\times 500$ dimers that has the same concentration (1%) but different configuration of the type-C defects compared to the system of the main simulation referred so far. The contour map of the local-order parameter at lower temperatures has a feature common to those of Figs. 5–8: the system is divided into three kinds of the mesoscopic regions, namely (+)-asymmetric, symmetric, and (−)-asymmetric regions. The sizes of the regions are about the same as the main simulation. Only the fraction of the area of the region is different from the main simulation in accordance with the configuration of the defects. Thus we conclude that the size of the system of the present simulation is large enough to show the essential feature of the structure of the local ordering. Values of the physical quantities depend rather on the configuration of the defects than on the size of the system so long as the mesoscopic regions are formed.

We also performed MC simulation for the system of 40 $\times 400$ dimers with the defect density of 2%. We see again that the three kinds of the mesoscopic regions are formed. The sizes of the regions are about the same as the system with 1% of defects. The LOP and the LEED intensity are much reduced at low temperatures as compared with the 1% type-C defect case. The transition of these physical quantities are more diffuse. We find that when the temperature dependence of the LEED intensity with coherence length $m=3$ is shifted to the lower side by about 80 K, it agrees well with the experimental result.[6] A larger coherence length is required to reproduce the experimental temperature dependence for the system of larger density of the defect. Thus, information about coherence length is necessary for analysis of the phase transition in terms of LEED. The middle point of the transition temperature region is little affected by increasing the defect density from 1 to 2%. As for the MOI, $Q_+ + Q_-$ becomes larger than that of the 1% type-C defect case at high temperature. At low temperature, $Q_+ + Q_-$ is almost the same as that of the 1% type-C defect case, while $|Q_+ - Q_-|$ becomes smaller than that of the 1% type-C defect case. The transition becomes more diffuse as well as that of the LOP and the LEED intensity.

V. CONCLUSIONS

We performed MC simulation to show how the LEED intensity and STM images change with temperature on Si(001) surface with defects and what is observed in LEED or STM on the surface. We introduced a low density (of 1% order) of the type-C defect, which is actually seen on the real surface. The order-disorder phase transition is much influenced by the defects. Compared with the defect-free system, the magnitude of the long-range-order parameter (LOP) is reduced at low temperatures and the temperature dependence of the LOP shows broad transition region. Formations of local domains at low temperatures are much influenced by the configurations of defects. It was clearly shown that different features of the low-temperature STM image by Wolkow[8] and by Tochihara, Amakusa, and Iwatsuki[9] can be observed on the same surface.

In the present study we proposed the fraction of the site of the asymmetric image, called ''mesoscopic ordering index (MOI),'' as a measure to describe the ordering of mesoscopic scale and showed its effectiveness in the quantitative analysis of the ordering from the STM image. As compared with the defect-free system, the temperature dependence of the MOI shows broad transition region. The local ordering is detected by an abrupt change in the temperature dependence of the local MOI. The transition becomes sharper with the reduction of the size of the region. The transition temperature differs from one local region to the other. This gives the reason why the transition of the total system with the defects of a low density becomes broad.

The temperature dependence of the LEED intensity shows broad transition region. The transition is seen more clearly for larger values of the coherence length of the incident electron beam. The dependence of the local LEED intensity on the coherence length is also investigated. Each local region begins to contribute to the total LEED intensity when the scale of the local ordering becomes larger than that of the coherence length. Therefore, we can get information about the scale of the local ordering from the dependence of the LEED intensity on the coherence length. Information about coherence length is thus necessary for analysis of the phase transition in terms of LEED. The experimental temperature dependence of the LEED peak[6] is explained as a combined effect of the defects and the coherence length.

The critical temperatures defined as the middle point of the transition region of the LOP, the MOI, and the LEED intensity are almost equal in the defect-free system and in the 1% type-C defect case. The present study offers an answer to the question what actually corresponds to the transitions observed in LEED and STM experiments.

ACKNOWLEDGMENTS

The MC simulation was performed at Research Institute for Applied Mechanics in Kyushu University through the courtesy of Professor E. Kuramoto.

*Corresponding author. FAX: +81-92-726-4740. Electronic address: nakayama@rc.kyushu-u.ac.jp

[1] D. J. Chadi, Phys. Rev. Lett. **43**, 43 (1979).

[2] K. Inoue, Y. Morikawa, K. Terakura, and M. Nakayama, in *Interatomic Potential and Structural Stability*, edited by K. Terakura and H. Akai (Springer, Berlin, 1993), p. 77.

[3] K. Inoue, Y. Morikawa, K. Terakura, and M. Nakayama, Phys. Rev. B **49**, 14 774 (1994).

[4] K. Terakura, T. Yamasaki, and Y. Morikawa, Phase Trans. **53**, 143 (1995).

[5] R. E. Schlier and H. E. Farnsworth, J. Chem. Phys. **30**, 917 (1959).

[6] T. Tabata, T. Aruga, and Y. Murata, Surf. Sci. **179**, L63 (1987).
[7] R. J. Hamers, R. M. Tromp, and J. E. Demuth, Phys. Rev. B **34**, 5343 (1986).
[8] R. A. Wolkow, Phys. Rev. Lett. **68**, 2636 (1992).
[9] H. Tochihara, T. Amakusa, and M. Iwatsuki, Phys. Rev. B **50**, 12 262 (1994).
[10] R. J. Hamers and U. K. Köhler, J. Vac. Sci. Technol. A **7**, 2854 (1989).
[11] T. Uda and K. Terakura, Phys. Rev. B **53**, 6999 (1996).
[12] T. Miyazaki, T. Uda, and K. Terakura, Mater. Sci. Eng. B **37**, 168 (1996).
[13] Y. Nakamura, H. Kawai, and M. Nakayama, Phys. Rev. B **52**, 8231 (1995).
[14] Z. Zhu, N. Shima, and M. Tsukada, Phys. Rev. B **40**, 11 868 (1989).
[15] Y. Imry and S. Ma, Phys. Rev. Lett. **35**, 1399 (1975).
[16] D. S. Fisher, G. M. Grinstein, and A. Khurana, Physics Today **41**, 56 (1988).